

MODELING AND ANALYSIS OF COMPOSITE SECTIONS WITH ARTIFICIAL PLY SEPARATION- APPLICATION IN HELICOPTER COMPONENTS

E. Ahci¹; M. Schulz²

¹Eurocopter Germany GmbH
81663 Munich, Germany
e-mail: elif.ahci@eurocopter.com

²P & Z Engineering GmbH
80939 Munich Germany
e-mail: martin.schulz@eurocopter.com

Key words: Rotor blade, separation foil, delamination

Abstract: Structural behavior of helicopter rotor blades is mainly driven by forced flapping and lead-lag bending deflections. By adding structural elements or reinforcing the main blade basic structure, these deflections create high forced stresses, which are difficult to manage. Therefore, a new design methodology was used to harmonize the stiffnesses by reducing the shear and especially the bending stiffness. By using separation foils it is possible to decouple the bending stiffness from the others. This method was used to create artificial delaminations of defined initial size.

Analytical and experimental investigations were performed to study the behavior of the composite laminates containing separation foils. The investigated design concept was applied in two different sub-parts of the main rotor blades.

A two dimensional finite element model was developed to predict the deformation form and the stress field acting along the separation front for a laminate of arbitrary thickness and stacking sequence, and a pre-introduced interlaminar separation of varying size and location.

Experimentally, thick-section E-glass fabric/epoxy laminated composite specimens containing separation foils between the layers were tested in three-point bending loading conditions to ascertain the behavior and dominant failure mode. In these tests the enforced displacements and the corresponding forces were measured. Additionally an analytical model has been created to get a correlation between the enforced displacements, measured force and delamination length.

Examples are presented to show the effect of number of separation foils on resulting critical delamination length. It was also shown by examples and experiments that the bending is the defining mode in the resulting deformation form.

1 INTRODUCTION

Fiber reinforced composite materials are being used to a greater extent for helicopter main rotor blades due to their increased stiffness and strength-to-weight ratio. By the use of fiber reinforced materials the main rotor heads are modified to eliminate the need for discrete flaps and lead-lag hinges. The recent developments in helicopter technology have introduced further simplifications into the rotor design. The consequence has been that more and more functions have been integrated into the rotor blade structures, resulting in increasing structural complexity.

The all-composite bearingless main rotor (BMR) of the EC 135 helicopter is a good example of a structurally complex and high technology design [1]. The details of the blade are shown in Figure 1. The BMR shows a 50 kg weight reduction and 40 % less part count compared to

the BO 105 rotor. The fully composite design (fiber glass and graphite epoxy) has characteristic fail-safe design features. The elastomeric dampers provide sufficient in-plane damping and the system of control cuff - flexbeam - control rod produces adequate pitch-lag coupling [2].

Whereas the rotor hub of the EC135 has an exceptionally simple design, the structure of the blade root has become rather complicated, as it has to take on the tasks of the hinges and bearings of a conventional rotor.

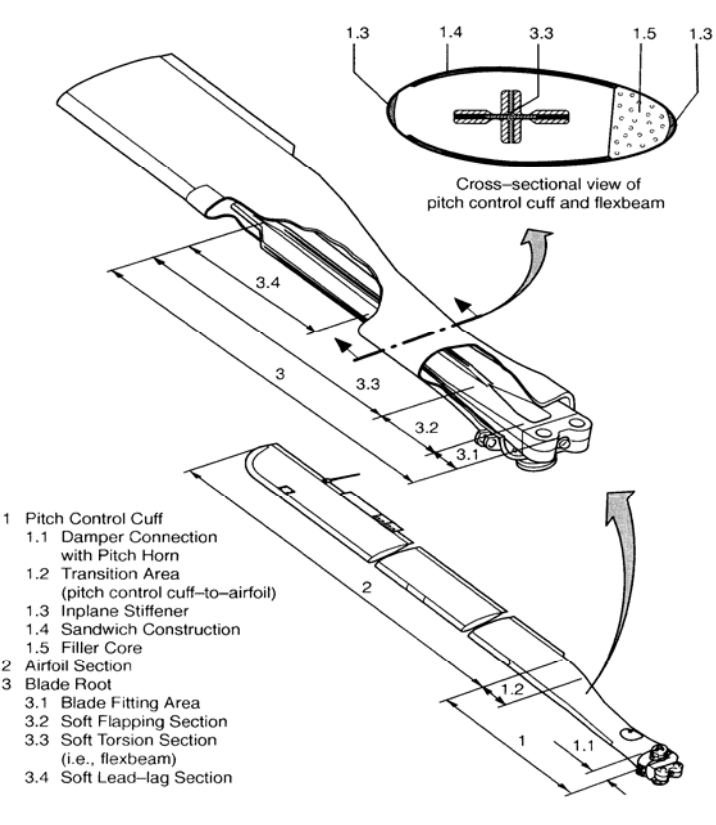


Figure 1: EC 135 bearingless main rotor blade including pitch control cuff, airfoil section and blade root

The key element of the rotor is the inboard portion of the spar, also called flexbeam. It connects the blade to the mast and has to carry all the primary flight loads. The main areas of the flexbeam are the blade attachment, followed by the tapered area, the “flapping hinge” section and the torsional element. Each section has its individual function, which is incorporated in a beam with minimum length in order to reduce the aerodynamic drag of the rotor. By use of the finite element method optimized cross sections were determined for torsionally soft flexbeam. Slits in the cruciform section remarkably reduce the torsional stiffness and the shear stresses due to the torsional angle and transverse loading. The trapezoidal flapping hinge cross section reduces the stresses due to the sum of lead-lag and flapping bending moments. The achieved design goals are minimum dimensions, maximum flapping flexibility with reasonable endurance limits and low shear stresses.

The EC 135 blade is entirely made up of fiber reinforced plastics with 135 °C epoxy resin system. Unidirectional tapes are used to carry the greatest part of the centrifugal force and the bending moments, whereas the $\pm 45^\circ$ layers in the shear web and the blade skin have to carry the greatest part of the shear loads including torsional moments. The composite control cuff

integrates with the airfoil skin and transfers the control inputs to the blade. Elastomer damping pads are attached on the inboard end of the control cuff to provide in plane damping. Main emphasis of the blade design was laid on the fail safe design features in order to meet the damage tolerance requirements of the Special Conditions of the Luftfahrtbundesamt (LBA).

2 DESIGN WITH ARTIFICIAL PLY SEPARATION

The structural elements or the reinforcements brought into the basic blade structure create high forced stresses and high displacements, which are difficult to cope with. Reducing the corresponding stiffness is one of the competent means to take care of these high stresses.

One part of the connection between the composite control cuff and the flexbeam are provided by the structural elements called C-profiles. Soon after, control cuff, flexbeam and blade skin integrate into the blade airfoil structure. Large bonding areas and the form locking design provides the load transfer. The complex loading condition and high relative displacements between the control cuff and the flexbeam require a special and sophisticated design.

The compound load transfer between the flexbeam and the control cuff principally defines the loading of the C-profiles. The flexbeam and the control cuff are loaded quite differently. The flexbeam is basically loaded by the centrifugal force, as well as the bending moments. The control cuff on the other hand, transfers the torsional moments to the homogeneous airfoil section and is additionally loaded by the bending moments and the compressive inertial forces. Part of the centrifugal force is transferred to the control cuff via C-profiles. Moreover, lead-lag and the flapping moments are transferred by means of the transition section including the C-profiles, which lead to transverse forces in C-profiles (Figure 2).

Furthermore, twisting angle between the flexbeam and the control cuff creates additional shear forces in the C-profiles. The effect of higher bending modes is negligible at the cross sections where the C-profiles are.

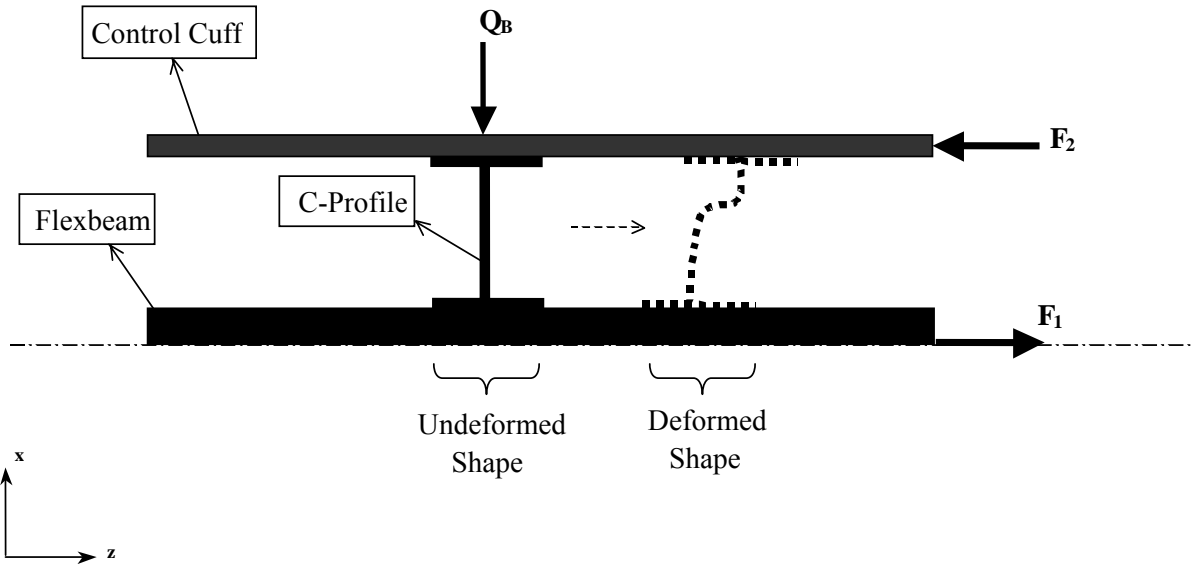


Figure 2: Principal sketch showing the loading of the connection elements –so called- “C-profiles” between the flexbeam and the control cuff

The C-profiles should be designed in such a way that the resultant design should carry the subsequent normal strains resulting from the centrifugal force transfer. On the other hand, the final construction should be stable in x-direction (Figure 2) to transfer the transverse forces. Therefore it is obligatory to have an optimized stiffness synchronization to manage the complicated loading situation. A special design with separation foils was used to harmonize the stiffnesses by reducing the shear and especially the bending stiffness. The proposed design solution decouples the bending stiffness from the others. Artificial delaminations of defined size were created using this method.

The new design concept is planned to be used in some structural parts of the EC 135 main rotor blades as a practical application. The current design of the C-profiles is planned to be improved and simplified by implementing the above mentioned design philosophy with separation foils. Preliminary experimental and analytical investigations were performed to clarify the behavior of a composite laminate containing the separation foils.

2.1 Theoretical Design Investigations

2.1.1 Delamination Behavior – Analytical Model

An analytical as well as a finite element model has been created to simulate the behavior of the laminate with separation foils. The analytical model combined with fracture mechanics provides a correlation between the enforced displacements, measured force (in the coupon tests, Chapter 2.2) and delamination length. Finite element model, on the other hand, was used to confirm the results of the analytical calculations and to clarify the computational modeling (e.g. element type used in meshing etc.) details, which were used later in the 3D finite element model of the real application.

A simple beam model representing the three point bending test specimens was created. The beam model consists of six sections with different stiffnesses and boundaries (Figure 3). In this figure, “L₂” and “L₁” are the lengths of the sections with and without the separation foils; “GA” is the shear stiffness; “EI” is the bending stiffness; “F_Q” is the transverse force and “Δu_z” is the imposed displacement. Both ends of the beam were kept fixed but free in x-direction to simulate the “S-shape” deformation form in a best way.

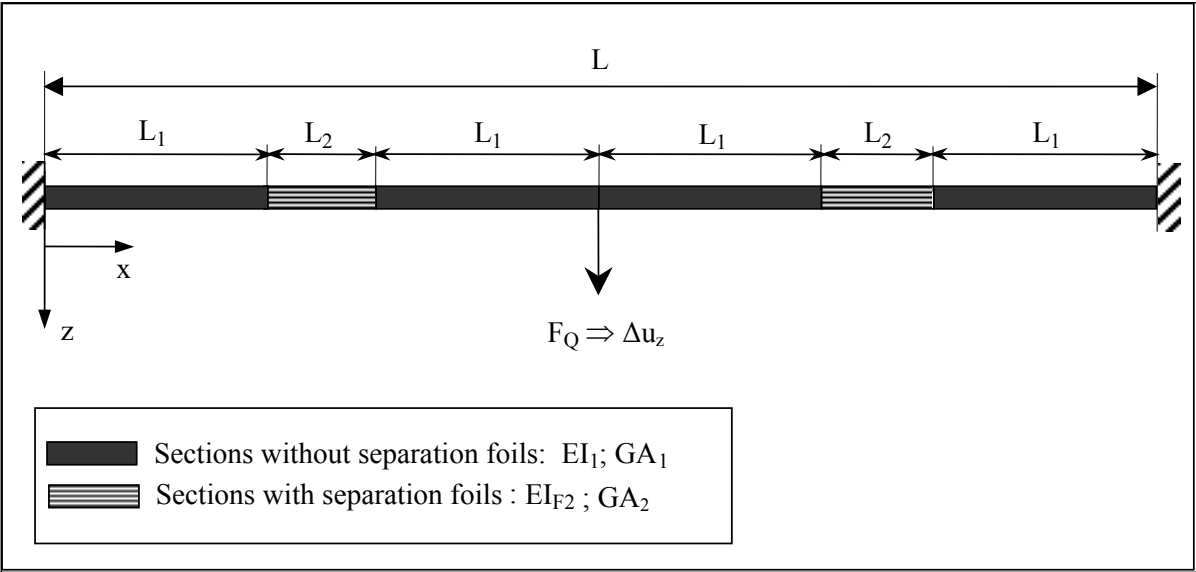


Figure 3: Sketch of the beam model showing the sections with and without separation foils

“ EI_1 ” in Figure 3 represents the bending stiffness of the section without separation foils. Similarly “ EI_{F2} ” is the bending stiffness of the section with separation foils:

$$EI_{bend} = EI_{F2} = EI_{plate} \cdot n_{plate} \quad (1)$$

“ EI_{F2} ”, represents the bending due to the transverse force. In this case the region with separation foils deforms in -so called- “S-shape” and the bending moment distribution is zero at the middle of the section with separation foils. “ EI_{F2} ” can be written as:

$$EI_{F2} = (n_{Foil} + 1) \cdot E_{fabric} \cdot \frac{b \cdot (t_{fabric} \cdot n_{layer})^3}{12} \quad (2)$$

“ n_{Foil} ” in Eqn. (2) is the number of separation foils, “ b ” is the width of the specimen, “ t_{fabric} ” is the layer thickness, “ n_{layer} ” is the number of fabric layers between the separation foils and “ E_{fabric} ” is the Young Modulus of the fabric layer.

The beam equation (3) defined for each one of the six sections (Figure 3) leads into a system of equations.

$$u_z'''(x) = \frac{-F_Q(x)}{EI} \quad (3)$$

The solutions of the system of beam equations are presented in Figure 4 - Figure 6. The system of equations was solved for two different cases to investigate the effect of number of separation foils on the resulting deformation form. Case 1 is the version with separation foils in between each layer of the laminate and case 2 is the version with separation foils between every three layers. The resultant global deformation due to the combined effect of bending and shear is given in Figure 4 for the case 1 and case 2. The “S-shape” deformation of the sections with separation foils can be seen clearly for both cases. It was initially assumed that the large relative displacement between the ends of the section with separation foils was defined by the shear stiffness of the system. In order to verify this hypothesis, the contribution of the bending and shear to the global deformation form was investigated separately.

The deformation form of the beam with separation foils due to bending and shear are shown in Figure 5 and Figure 6 respectively.

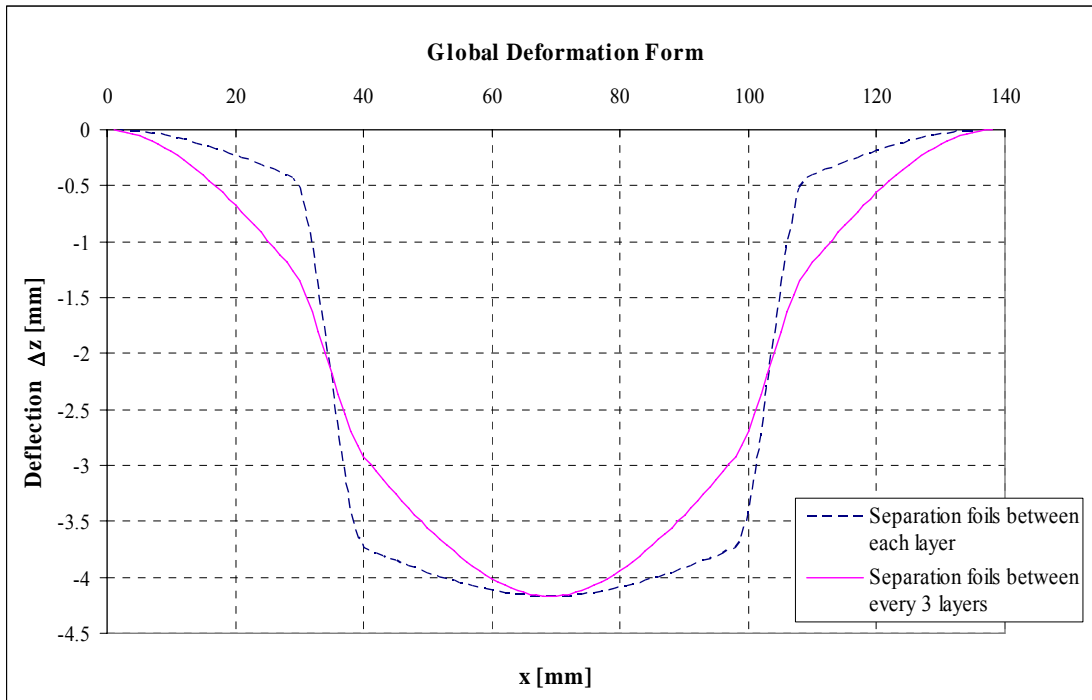


Figure 4: Total deformation of the beam (Δz) with sections having separation foils between the fabric layers due to shear and bending

Figure 5 and Figure 6 show undoubtedly that the contribution of shear to the resultant deformation is negligible. It is clear that high relative displacements occur due to the different bending stiffnesses of the sections with and without separation foils. The final deformation form -explicitly the large deflection between the ends of the section with separation foils- is defined by the relatively low bending stiffness of the section compared to the other sections without separation foils. The shear and bending stiffnesses used in the beam model were given in Table 1.

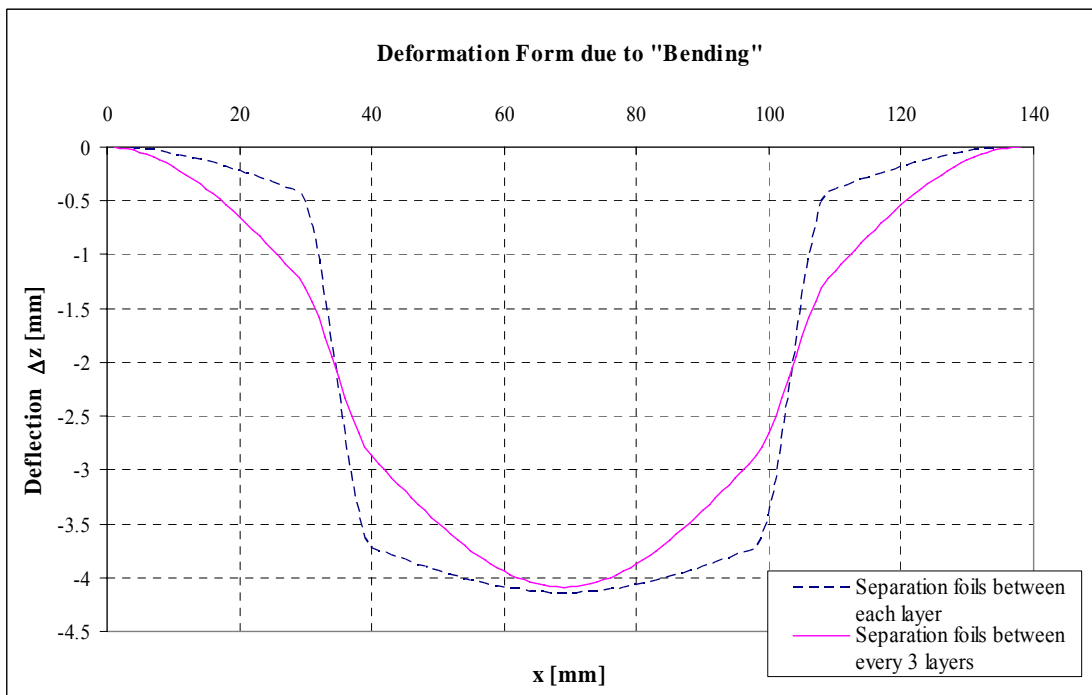


Figure 5: Bending deformation of the beam with sections having separation foils between the fabric layers

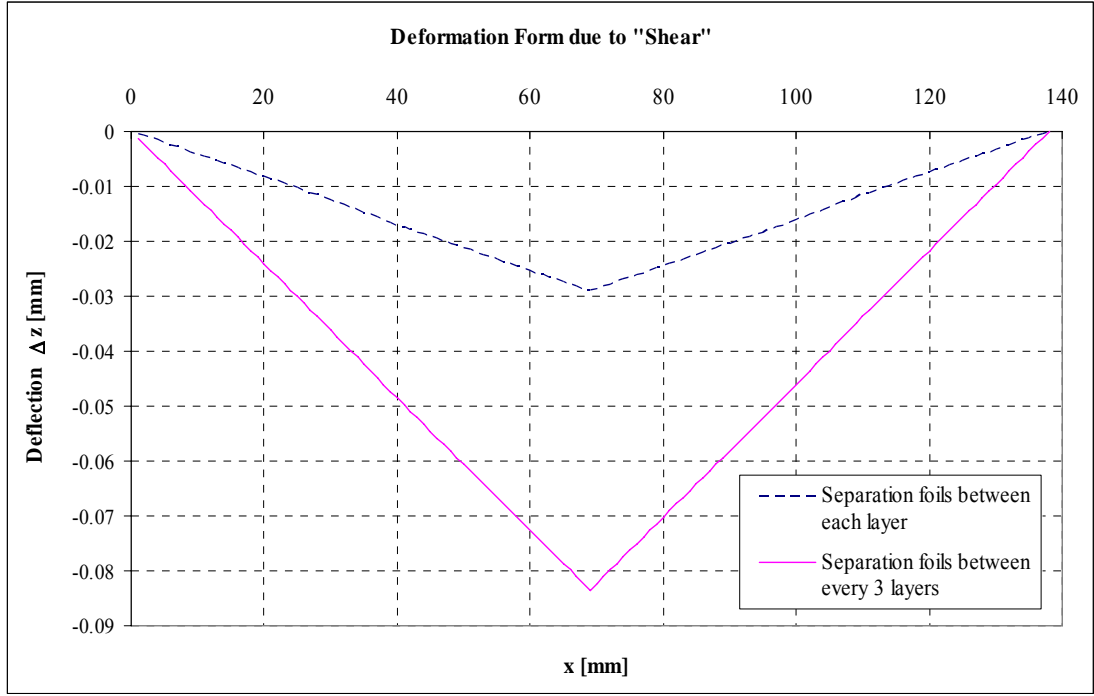


Figure 6: Shear deformation of the beam with sections having separation foils between the fabric layers

| Remarks | Bending stiffness [N.mm ²] | Shear stiffness [N] |
|--------------------------|---|--------------------------|
| Without separation foils | $EI_1 = 4.7 \cdot 10^6$ | $GA_1 = 4.57 \cdot 10^5$ |
| With separation foils | $EI_{F2} = 6.75 \cdot 10^4$ | $GA_2 = 4.44 \cdot 10^5$ |

Table 1: Stiffnesses used in the beam model (Figure 3)

The dominant mode, i.e. bending or shear, in terms of resultant deformation form can also be identified by examining the stiffnesses determined for the sections with and without foils (Table 1). The shear stiffnesses of the sections with and without separation foils (i.e. GA_2 and GA_1 in Figure 3) are almost the same. The bending stiffness of the section with foils, “ EI_{F2} ” on the other hand, is relatively low compared to the one for the section without foils, “ EI_1 ”. After the determination of the deformations due to bending and shear, the resultant strain $\varepsilon_x(x,z)$ distribution was calculated. Strain energy “ Π ” and the strain energy release rate “ G_{II} ” were determined afterwards at the position $x = L_1$ according to fracture mechanics [3]:

$$\Pi = \frac{1}{2} \cdot E_{fab} \cdot \int \varepsilon_x(x,z) dV \quad (4)$$

$$G_{II} = \frac{\Pi_I - \Pi_{II}}{n_{Tedlar} \cdot \delta a \cdot b} \quad (5)$$

In Eqn. (5), “ Π_I ” is the strain energy of the section with separation foils and similarly “ Π_{II} ” is the strain energy of the section without foils; δa is the integration range in x-direction representing the delamination length.

During the experimental program, three point bending tests specimens were tested dynamically and loaded with different enforced displacements (explained in chapter 2.2). For a defined displacement, the resultant transverse force “ F_Q ” and the strain energy release rate “ $G_{II,max}$ ” for the maximum deflection was determined theoretically from Eqn.s (4) and (5) together with the beam model.

Varying the length of the section with separation foils in the analytical model it was shown that a delamination length of 0.5 mm at each end of the foils leads to 4% decrease in the transverse force. This value and the corresponding change in the transverse force are realistic in the sense that they can be measured in the experiments. Therefore, the delamination length of 0.5 mm was assumed to be the initiation of the delamination at the ends of the separation foils.

2.1.2 Finite Element Model

Finite element analyses were performed to verify the predictions of the analytical model, especially the deformation form and the contribution of the bending to the overall deflections. A three dimensional finite element model was created in NASTRAN for this purpose. The modeling details such as the element type to be used to represent the behavior of the laminate with foils realistically have provided the bases for the FEM analysis performed for the real example, i.e. C-profiles of the EC 135 main rotor blade.

The determined deformation by using finite element analysis is presented in Figure 7. “S-shape” deformation form can be seen clearly along the section having separation foils in between the layers. The defining role of the bending stiffness in the resulting “S-shape” deformation was confirmed by the finite element analysis. The results of the finite element analysis have a good agreement with the analytical predictions. The details of these calculations are not given in this paper to focus more on the experimental investigations and the studies performed for the practical application.

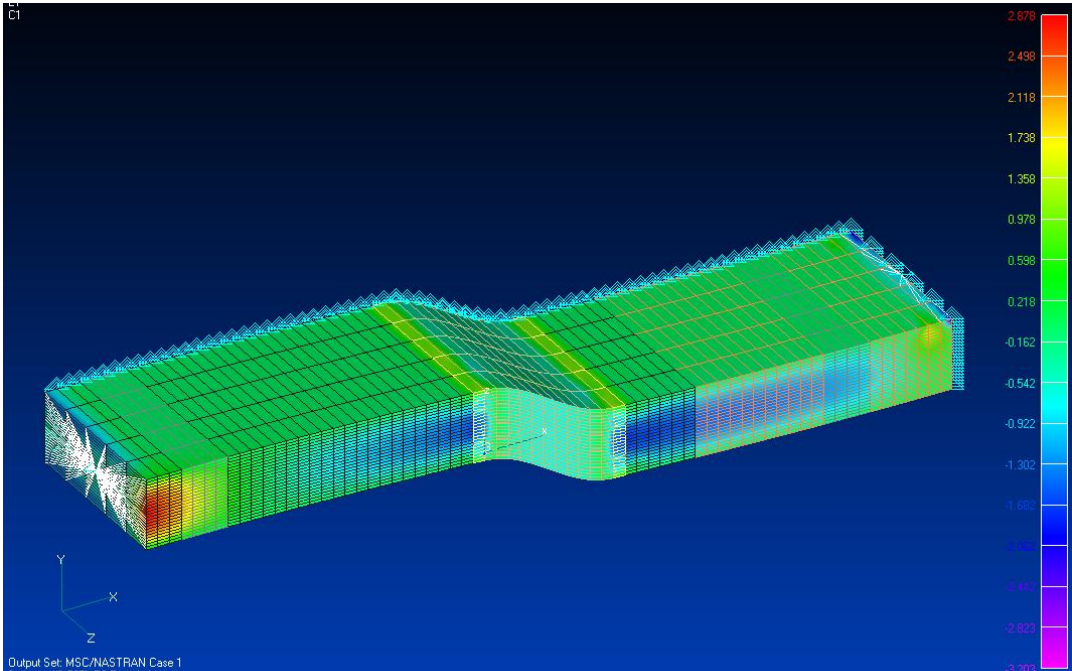


Figure 7: Predicted deformation of a composite beam with a section having separation foils

2.2 Experimental Design Investigations

Three point bending tests were performed with thick-section E-glass epoxy specimens with separation foils in between the layers to ascertain the behavior and the dominant failure mode. The main purpose of the tests was to determine the shear and bending characteristics (e.g. strength, stiffness and the deformation form) of the laminates with separation foils. Loading conditions of the C-profiles, i.e. the resultant normal strains in the C-profiles due to limit loads in practice, have been simulated.

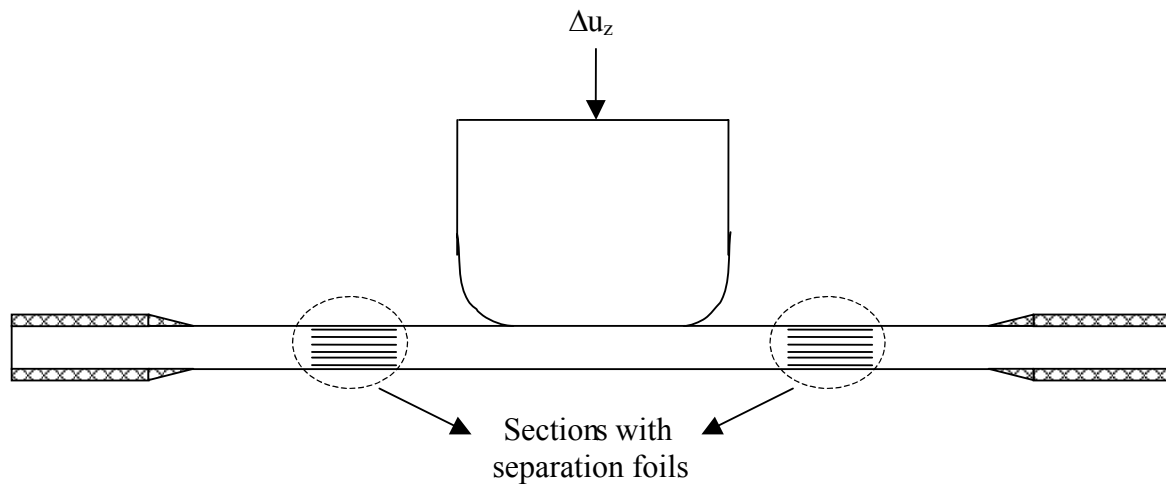


Figure 8: Simple sketch of the three point bending test specimen showing the position of the separation foils

Three point bending specimens were manufactured according to an Eurocopter standard. The specimens were approximately 180 mm long and 6 mm thick (Figure 8). Moments had to be fixed at both ends of the specimens to simulate the “S-Shape” deformation. The test set-up has been modified for this purpose.

Two different configurations of specimens with separation foils in between each layer and in between every three layers were tested to investigate the effect of number of foils. Static and dynamic three point bending specimens were tested on a regular pulsar test machine at room temperature. Dynamic tests were performed as displacement controlled. The relative displacement between the control cuff and the flexbeam of the EC 135 blade resulting from the centrifugal force, flapping and lead-lag moments was defined as the enforced displacement in these tests (“ Δu_z ” in Figure 8). The imposed displacements in the dynamic tests were defined at limit load or higher levels (Figure 9).

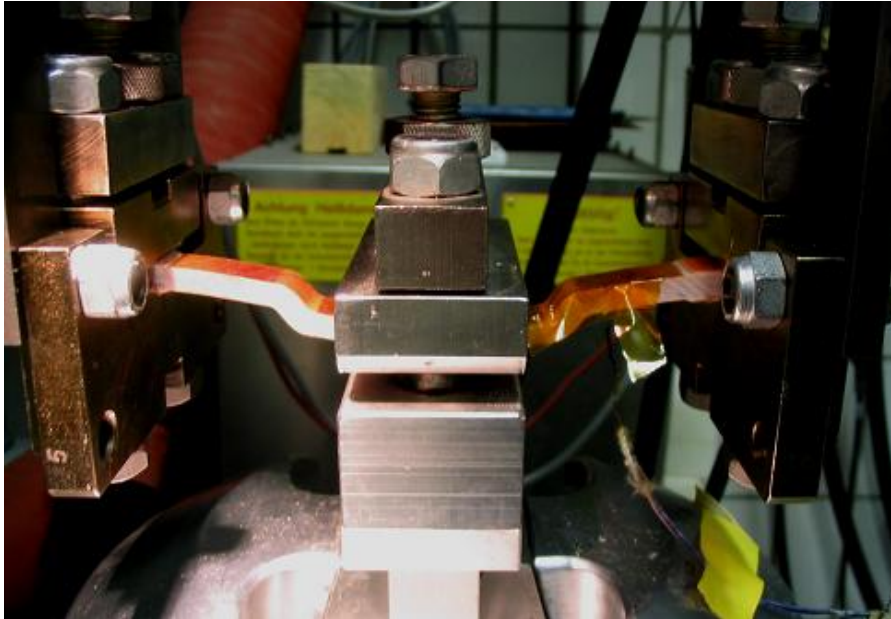


Figure 9: Three point bending test specimen having separation foils between the layers along the areas deformed in “S-shape”

Static tests were performed initially. Static loads were increased as much as possible until the limitations defined by the test set-up. The specimens were loaded gradually and the enforced displacements and the corresponding forces were measured simultaneously (Figure 10). Following the resultant 10 mm deflection, the measured force started to decrease (Figure 10). This indicates that the layers, which have foils in between them starts to separate from each other and afterwards delaminations begin at the ends of the foils. Static tests were continued up to a level at which the measured deflection was 20 mm. It is important to mention that the maximum displacement at the C-profiles resulting from the operational loads in practice is 0.72 mm (limit load value). At the ends of the static loading only delaminations were observed at both ends of the foils, but there was no rupture of the specimens.

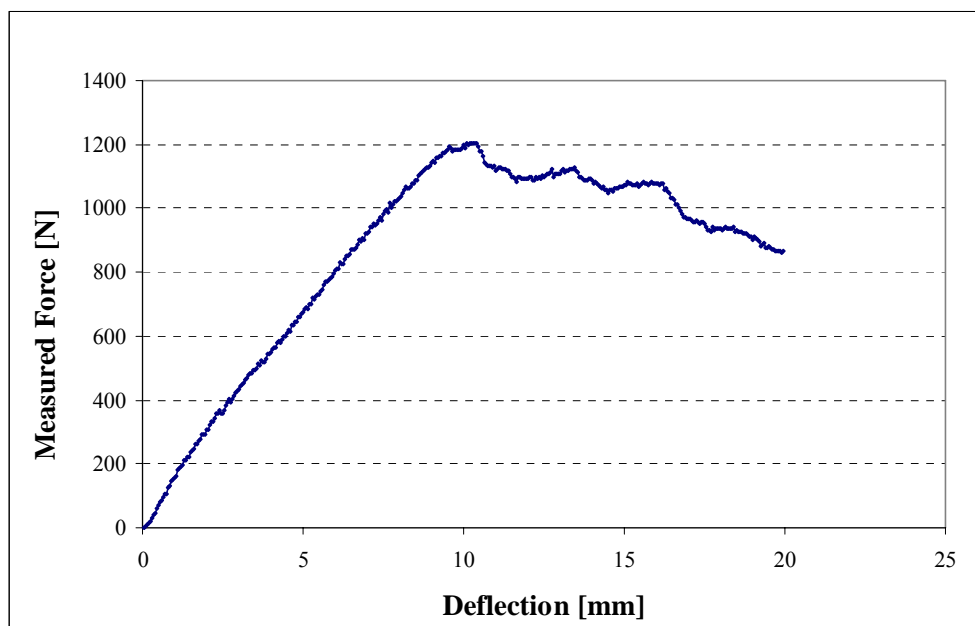


Figure 10: Measured transverse force and the corresponding deflection recorded for a three point bending test specimen loaded statically (Case 2: Separation foils between every three layers)

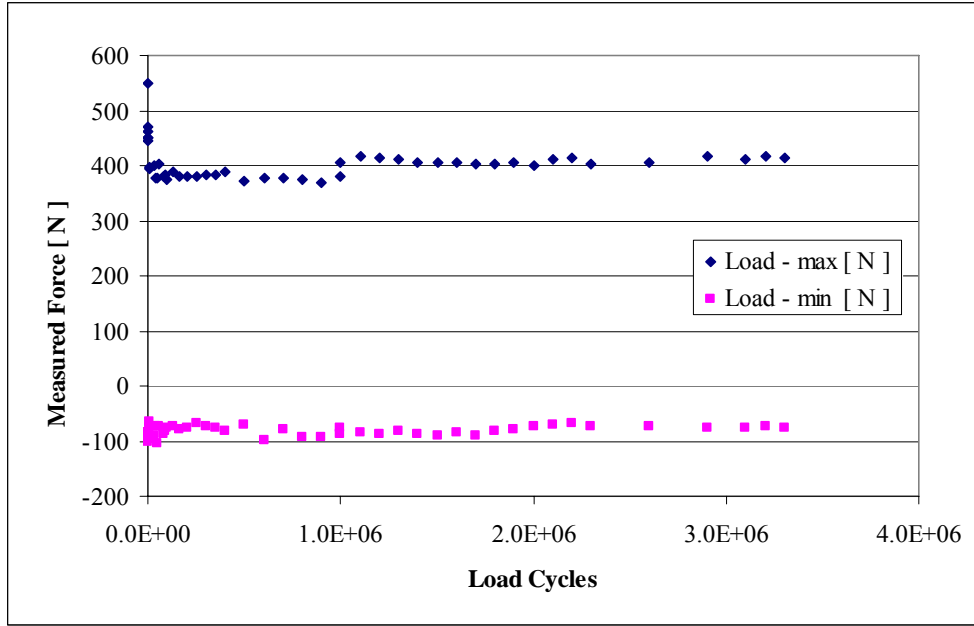


Figure 11: Measured transverse force versus the number of load cycles recorded for a three point bending test specimen loaded dynamically (Case 2: Separation foils between every three layers; $\Delta u_z = 3 \text{ mm} / -0.3\text{mm}$; $f = 3\text{Hz} / 6\text{Hz}$)

Identical measurements were performed for the dynamic tests. An example of the measurement results is presented in Figure 11. The decrease in the measured force after the first 400 load cycles indicates that the layers, which have foils between them, separate from each other. The experimental results were compared with the analytical predictions later on. As mentioned in Chapter 2.1, delamination length of 0.5 mm and the corresponding 4% decrease in the transverse force have been defined as the delamination initiation at both ends of the sections with separation foils. Except for the initial drop caused by the disconnection of the layers, no further decrease of 4% in the measured force has been detected.

As mentioned earlier, it was requested to fix the moments at both ends of the specimens to simulate the “S-Shape” deformation. But it has been seen during the tests that one end of the specimens was not entirely fixed even though the test set-up was modified for this purpose. This end was not completely rotation free but some condition between entirely fixed and totally rotation free end conditions. Therefore the analytical model was modified to consider this effect and as a conservative approach it was assumed that one end is completely rotation free (Figure 12).

Accordingly the bending stiffness of the section with separation foils was modified and consists of two different parts now:

$$EI_{bend} = EI_{F2} + EI_{M2} = EI_{plate} \cdot n_{plate} + \sum_{i=1}^{n_{plate}} A_i \cdot z_{m,i}^2 \quad (6)$$

The first part, “ EI_{F2} ”, represents the bending due to the transverse force as before. The second part, “ EI_{M2} ”, is the -so called-”Steiner Part”, i.e. the part representing the transverse force free bending. That means, for the bending due to the transverse force, the factor “ Az^2 ” (Steiner Part) should not be included in the stiffness calculations. “ EI_{M2} ” was calculated as $4.54 \cdot 10^6 \text{ [N.mm}^2\text{]}$. Due to the fact that “ EI_{F2} ” is approximately 100 times less than “ EI_{M2} ” the main part of the deformation is still defined by the bending of the each package¹.

¹ “Package” means the sum of fabric layers in between the separation foils

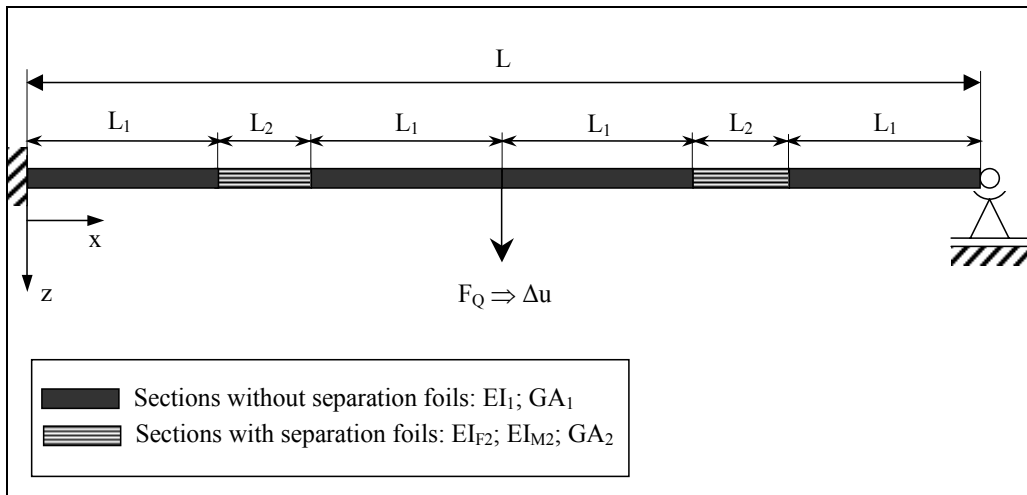


Figure 12: Sketch of the beam model showing the sections with and without separation foils

The resultant deformation due to shear and bending was recalculated according to the modified formulation derived by considering the new end conditions. The results are presented in Figure 13. The contribution of shear to the total deformation is almost zero. The “S-shape” form of the deformation can be clearly seen between the ends of both regions (along the length “ L_2 ” in Figure 12) with separation foils in between the layers.

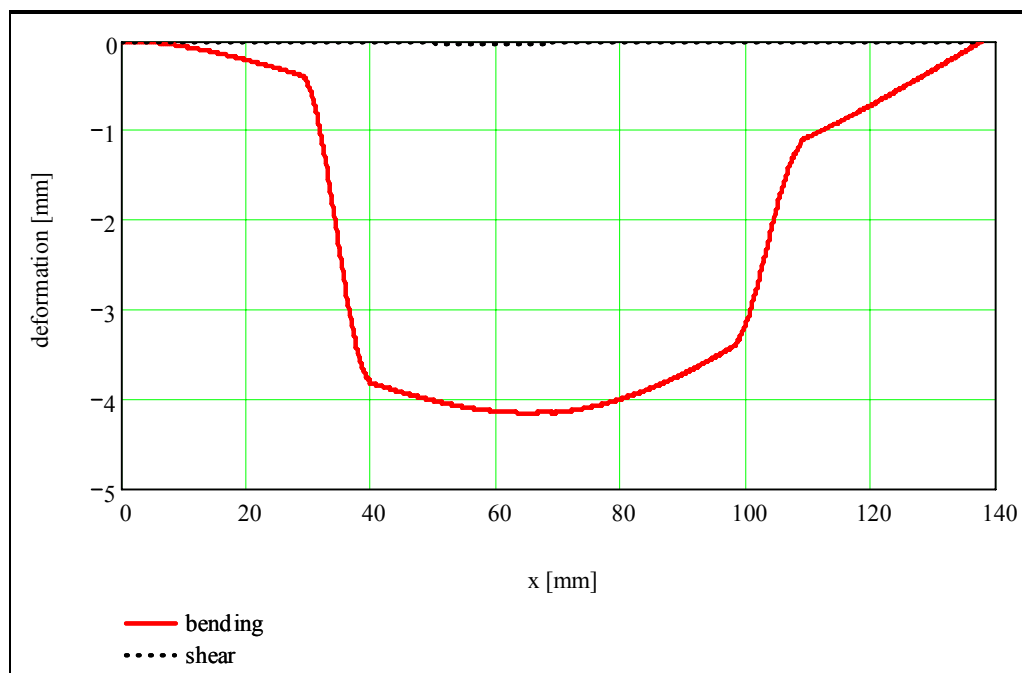


Figure 13: Deformation of the beam model due to shear and bending

3 PRACTICAL APPLICATION OF THE PROPOSED NEW DESIGN

After the preliminary analytical and experimental analysis, the proposed design philosophy was implemented to the real application, i.e. the design of the C-profiles was modified following the new design principles. C-profile walls, i.e. webs, include separation foils between every three layers after the new design adaptation (Figure 14). It was decided to place the separation foils in between every three layers due to the required stability in x-direction (Figure 2) to carry the transverse forces resulting from the lead-lag and the flapping moments transferred via C-profiles.

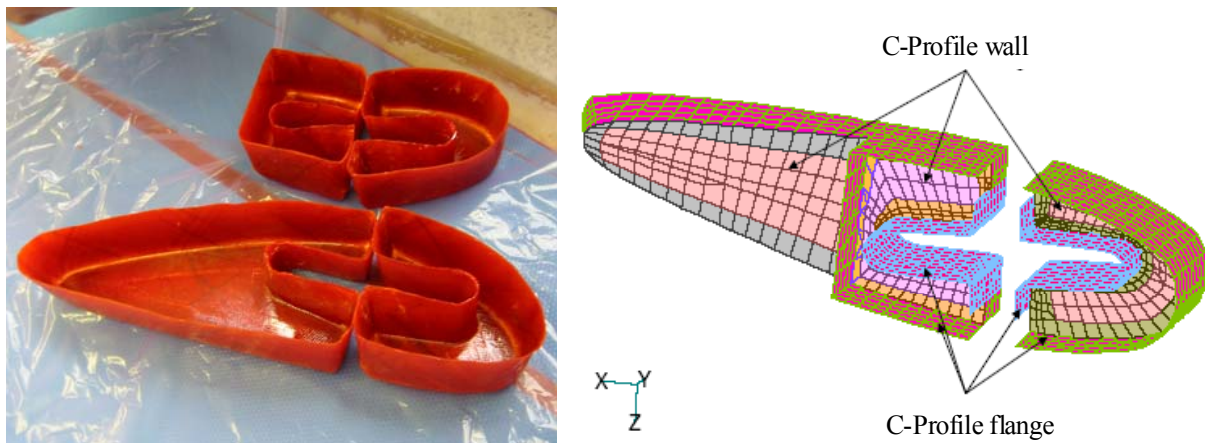


Figure 14: Photo showing the C-profiles manufactured with separation foils and a principle sketch showing the web and flange sections of the C-profiles

Computational and experimental analyses were carried out to study the practical implementation of the new design concept in detail. For this purpose simple analytical calculations as well as 3-D finite element analysis have been performed. To facilitate the design process CATIA 3-D computer aided design tool was used as the design medium. The design of the structural components, i.e. C-profiles, were created in 3-D models and transferred to NASTRAN for finite element analysis. This process enabled the structural components to be optimized for the required static and fatigue strength with minimum weight impact. At last, the finalized design state has been demonstrated in the small specimens and tested statically and dynamically.

3.1 Theoretical Investigations

3.1.1 Delamination Behavior of the C-Profiles

The correlation between the load spectra in flight and the strain energy release rate was established to analyze the risk of delamination in the C-profiles

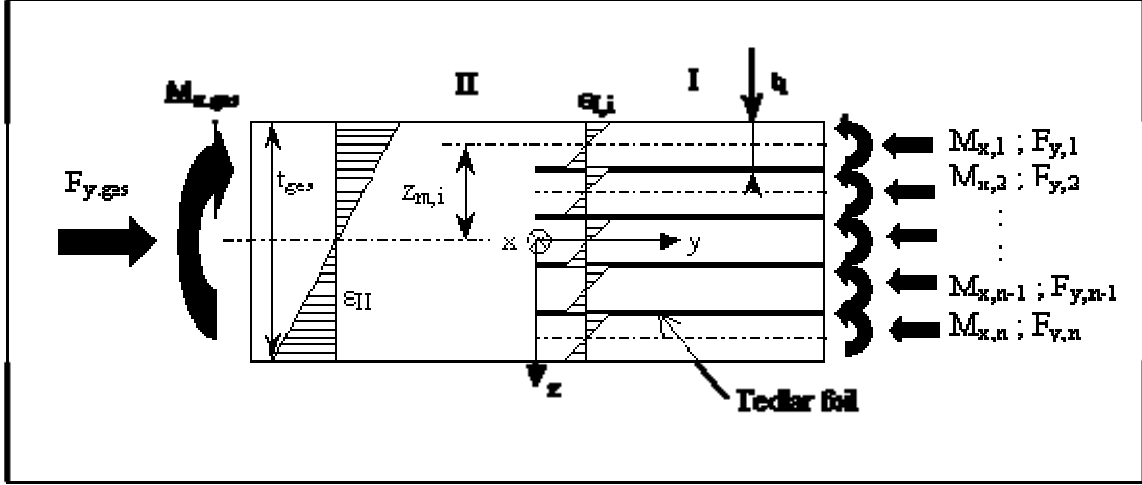


Figure 15: Load and stress situation of a beam structure including separation foils

Figure 15 shows the model that was used to calculate the strain energy release rate at the transition area between the laminates with and without separation foils. Then, Eqn. (4) leads to

$$\Pi_I = \frac{1}{2} \sum_i \cdot \int_{-\frac{t_i}{2}}^{\frac{t_i}{2}} \left(\frac{144 \cdot M_{x,i}^2}{E_i \cdot b \cdot t_i^6} \cdot z^2 \cdot \delta a \right) dz + \frac{1}{2} \frac{\sum_i (F_{y,i})^2 \cdot \delta a}{E_i \cdot b \cdot t_i} \quad (7)$$

$$\Pi_{II} = \frac{1}{2} \cdot \int_{-\frac{t_{ges}}{2}}^{\frac{t_{ges}}{2}} \left(\frac{144 \cdot \left(\sum_i M_{x,i} + F_{y,i} \cdot z_{m,i} \right)^2}{E_{ges} \cdot b \cdot t_{ges}^6} \cdot z^2 \cdot \delta a \cdot b \right) dz + \frac{1}{2} \cdot \frac{\left(\sum_i F_{y,i} \right)^2 \cdot \delta a}{E_{ges} \cdot b \cdot t_{ges}} \quad (8)$$

By substituting the Eqn.s (6) and (7) back into the Eqn. (5), the corresponding strain energy release rate was determined.

To get the correlation between the flight loads and the strain energy release rate, free body loads determined from the finite element model were used in the strain energy release rate equation. The nodes representing the transition between the area with and without separation foils were selected to obtain the free body loads. These nodes are located at the region with highest strains occurring as a result of limit loads. In total eight nodes were used. There are bending moments and normal forces due to centrifugal force, lead-lag and flapping moments. So the resulting moment $M_{x,i}$ and the force $F_{x,i}$ on the i -th node is given as:

$$M_{x,i} = M_{x,\text{centrifugal_force}} + M_{x,\text{lead_lag}} + M_{x,\text{flapping}}$$

$$F_{y,i} = F_{y,\text{centrifugal_force}} + F_{y,\text{lead_lag}} + F_{y,\text{flapping}}$$

The moments and forces due to different load cases were normalized to the corresponding loads at the blade bolts. The measured flight loads were also transferred to this radius station by using the conversion factors. The corresponding limit values of the flapping and lead-lag moments and the centrifugal force at this radius station gives the maximum strain energy release rate of $G_{II,\text{max}} = 308 \text{ N/m}$. Using the critical strain energy release rate of $G_{II,\text{cr}} = 1101 \text{ N/m}$ [3] defined for the E-Glass/913 material system, the margin of safety concerning the instantaneous delamination was determined as 0.83.

It has to be mentioned that delamination at the ends of the separation foils is not the failure of the C-profiles. C-profiles become less stiff due to the delaminations and therefore the bending moments reduce, as well as the strain energy release rate.

3.1.2 Finite Element Analysis

Due to the separation foils in between the layers of vertical walls (i.e. webs) of the C-profiles, they behave like a pack of single plates fixed together at both ends. So, when this pack is bent with an “S-shape” form as explained in Chapter 2, the bending stiffness $EI_{\text{S-shape}}$ can be determined as follows:

$$EI_{\text{S-shape}} = EI_{\text{plate}} \cdot n_{\text{plate}} \quad (9)$$

Therefore, in order to simulate this behavior, the webs of the C-profiles with separation foils were simulated as a pack of eight walls next to each other in spanwise direction (Figure 16). Each wall simulates the laminate between the separation foils. These walls were connected to the elements representing the flange sections of the C-profiles (Figure 14). This modeling technique was confirmed by the preliminary FEM analysis performed for the three point bending specimens.

The structure of the laminate was defined by PCOMP property card in NASTRAN. The property ID as well as the material definition, layer thicknesses and the fiber orientation angles were defined in this property card.

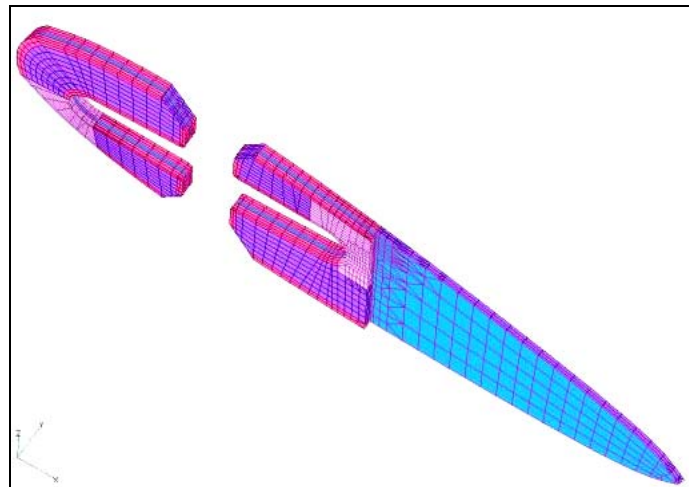


Figure 16: Finite element mesh of the C-profiles as a pack of adjacent walls

The structure of the finite element model is shown in Figure 17. It consists of beam, shell and volume elements as well as concentrated mass elements. The flexbeam, control cuff, and skin outside the considered range as well as the control rod and the lead-lag damper were represented by mass points and beam elements. The transition region (i.e. C-profiles, foam parts etc.) between the flexbeam and the control cuff were represented three dimensionally with shell and volume elements. The transition between the beam elements and the three dimensional part was simulated by rigid body elements.

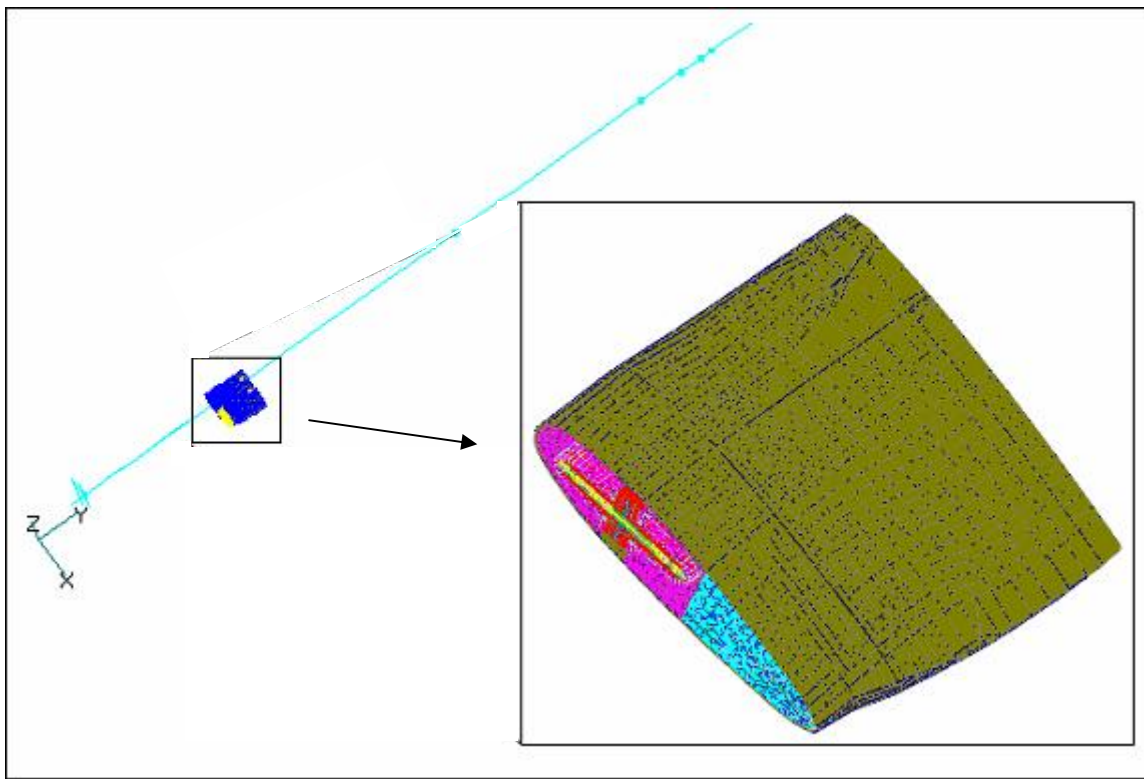


Figure 17: Finite element model showing the beam, shell and volume elements used to represent flexbeam, blade skin, control cuff and transition region between them

The mass of the real structure was assigned to the beam elements as distributed weight per unit length. Additionally, the material card used for the shell and volume elements contains the density information. By this way the mass distribution in the model matches up with the reality. Centrifugal force was produced over the rotation of the model around the z-axis (Figure 17). The maximum flight load cases for the flexbeam and the control cuff occur with a rotor speed of 6.85/s. That corresponds to 104% of the rated speed. The loads for the flapping and the lead-lag were originated from the first Eigenmodes. In order to determine the resultant bending moments modal analysis was accomplished. Finally, analyses were performed for the combined load case including the centrifugal force, flapping and lead-lag moments and torsion. Additionally, the twisting between the flexbeam and the control cuff was also introduced in the model.

The deformed shape of a single C-profile is shown in Figure 18. The “S-shape” deformations at the edges can be seen very nicely.

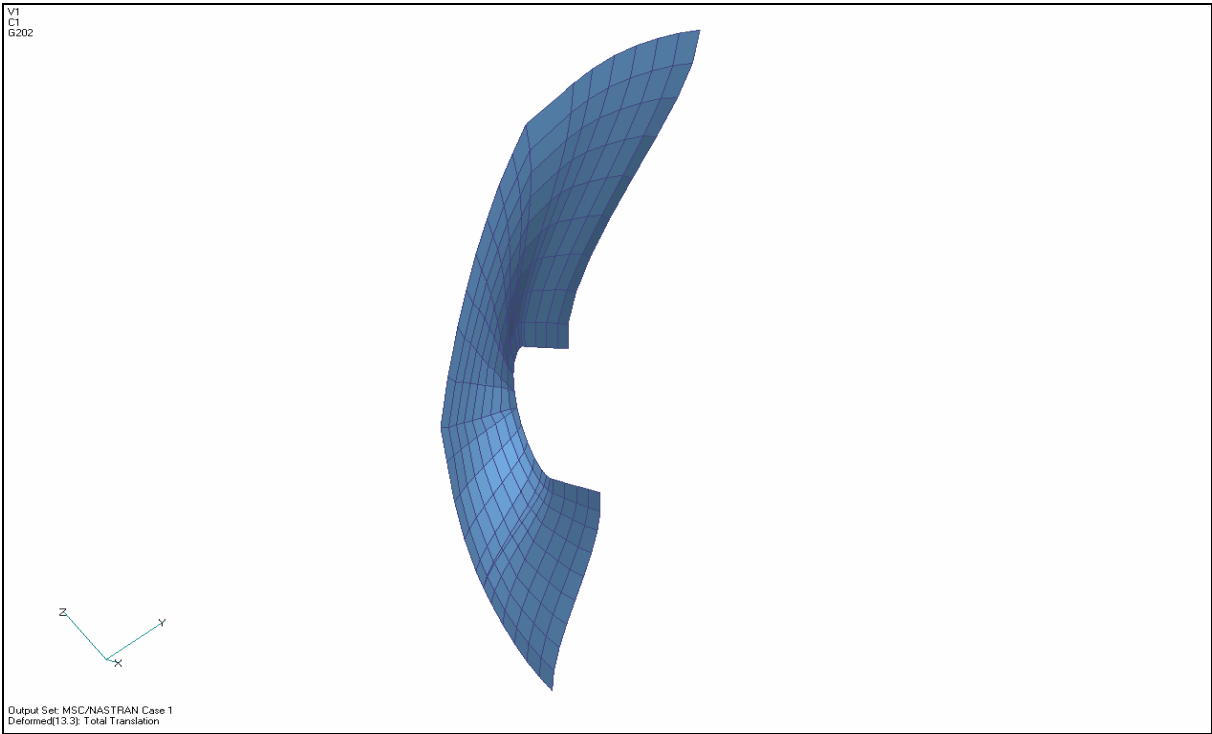


Figure 18: Deformed shape of the C-profiles under the combined load case, i.e. centrifugal force, flapping and lead-lag moments and torsion

3.2 Experimental Investigations: “Donut Tests”

The final design configuration, i.e. the geometry and the construction details of the connection elements, were simulated in the -so called- “Donut Specimens” (Figure 19). “Donut” specimens were manufactured according to the serial manufacturing principles in terms of the number of layers, the lay-up sequence and the position of the separation foils. Then, the specimens were tested with the help of a special test apparatus to reproduce the complex loading of the C-profiles.



Figure 19: “Donut” Specimens: Front/rear views and two specimens next to each other

The specimens were manufactured from E-Glass fabrics and in between every 3 layers there was one layer of separation foil. As a first step, each specimen was bonded to the inner and outer rings to prevent the relative displacement against these rings under effect of loading (Figure 20). The pair of specimens were held together by means of a spindle and placed into the housing. After the bonding, two specimens were tested together as a single unit (Figure 21).

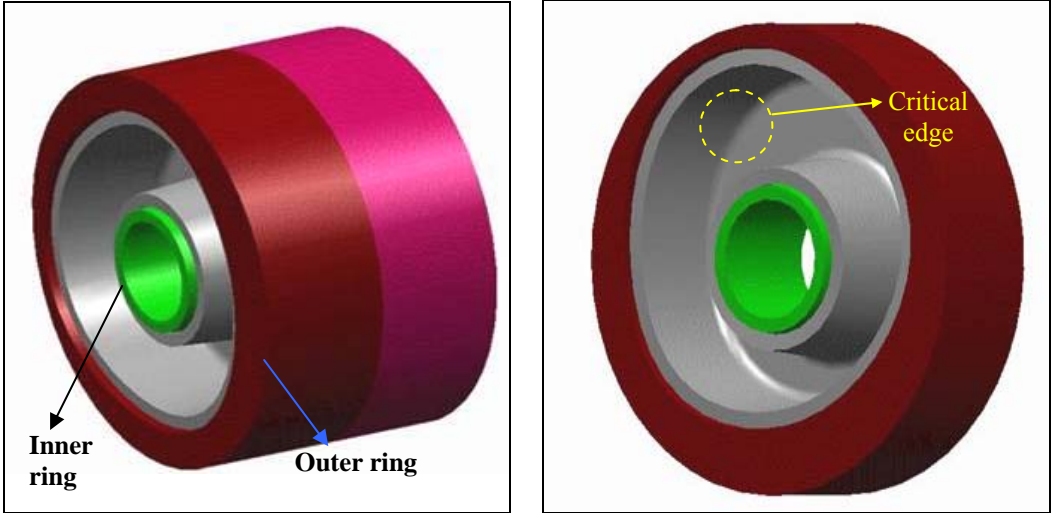


Figure 20: Principle sketches showing the “Donut” specimens as a pair and the critical edge



Figure 21: Photo of the test apparatus with specimens already placed into the housing

Besides specimens with separation foils, specimens without foils were tested as well to the same specs to investigate the difference in terms of stiffness. Static and dynamic tests were performed with the help of a special test apparatus, which was mounted to the regular pulsing test machine. Dynamic tests were performed on conditioned and unconditioned specimens at room temperature. The relative displacement between the control cuff and the flexbeam due to centrifugal force, flapping and lead-lag moments was defined as the enforced displacement in these tests. These displacements were defined at limit load or higher levels.

First static tests were performed. Static loading was increased as much as possible until the limitations defined by the test set-up. The specimens were loaded gradually and, the enforced displacements and the corresponding forces were measured simultaneously. Similar measurements were also performed for the dynamic tests. An example of the measurement results is presented in Figure 22. The decrease in the measured force after ~4000 load cycles (for specimen number 3 in Figure 22) occurs basically due to the fact that the layers having foils between them separate from each other. Conversely, on specimens without foil separation the decrease in measured force continues through the end of the test until failure occurs. The reason for this behavior is the higher stiffness of the specimens without foils compared to the ones with foils. Except for the initial fall caused by the disconnection of the layers, no further decrease in the measured force has been observed for the specimen with foils.

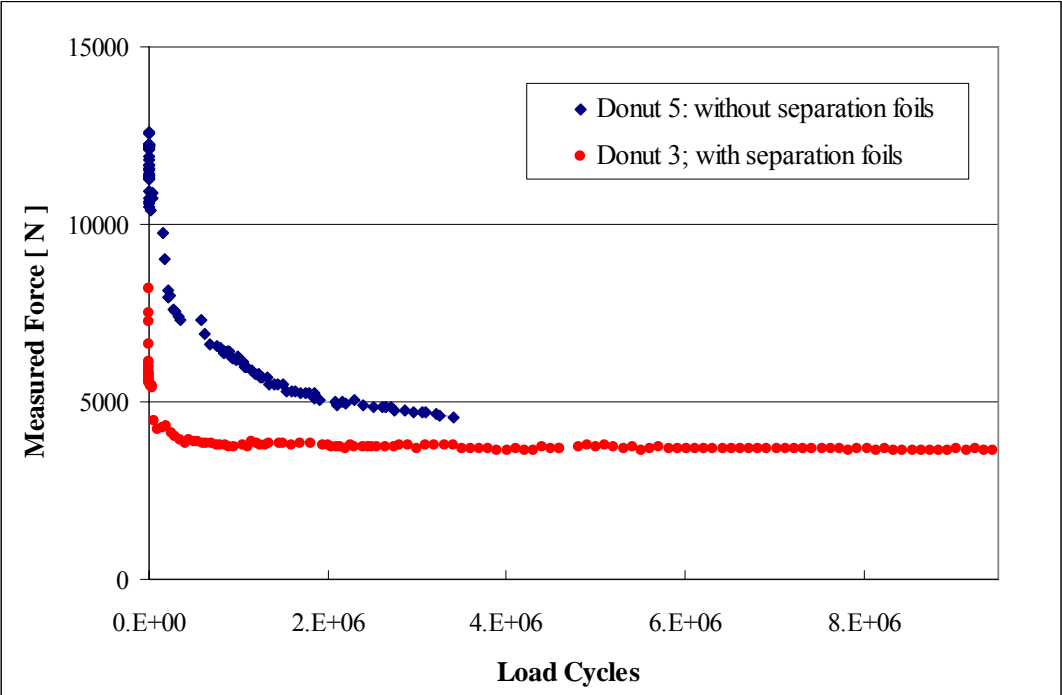


Figure 22: Measured transverse force versus the number of load cycles for “Donut” specimens with and without separation foils ($\Delta u_z = 1.03 \text{ mm} / - 0.104 \text{ mm}$; $f = 3 \text{ Hz} / 6 \text{ Hz}$)

Specimen number 3 with separation foils has been dynamically loaded for 9 million load cycles with maximum enforced displacement of 1.03 mm. During the test with the help of an endoscope the condition of the critical edge between the web and the flange section² of the “Donut” specimens (Figure 20) was inspected. The photos made by using an endoscope towards the end of the test are shown in Figure 23. It can clearly be seen that delaminations have appeared at the edge of the “Donut” specimens.

² The bottom and the vertical surfaces of the „Donut“ specimens are named „Web“ and „flange“ sections respectively

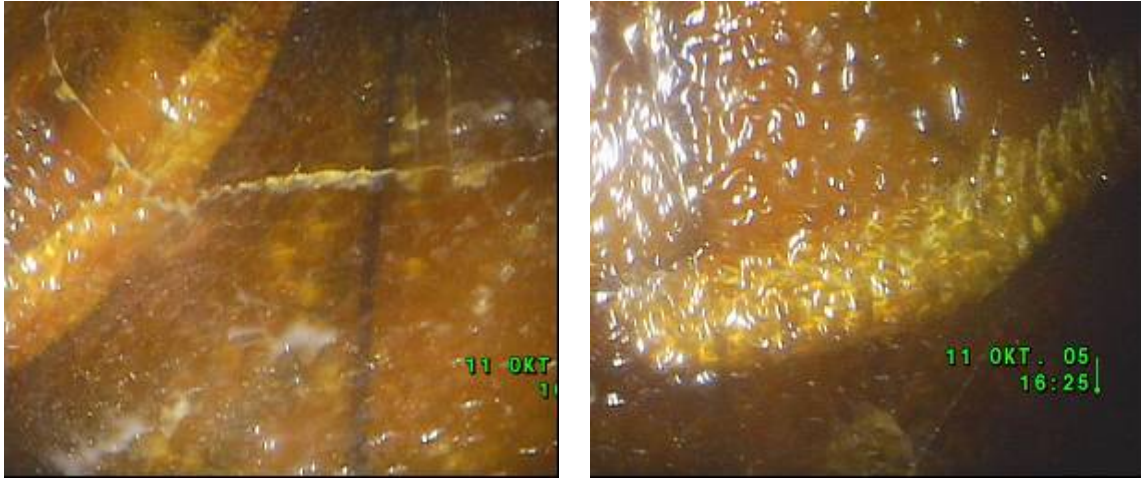


Figure 23: Endoscopic pictures of the “Donut” specimens taken from the edge between the web and the flange sections

After 9 million load cycles, the specimen pairs were removed from the test apparatus and the status of the composite structure was visually examined. It was detected that the specimens without separation foils were entirely cracked in the web section (Figure 24). On the other hand, no cracks were observed in the specimens having separation foils in between the layers. This result confirms the improvements gained by the new design concept, i.e. the reduced bending stiffness.



Figure 24: Photo showing the status of the “Donut” specimens with and without separation foils after the dynamic test

4 SUMMARY

The bending and shear stiffness of a laminate was optimized by introducing the foil separation concept to carry high deflections. This new design philosophy basically reduces the shear and particularly the bending stiffness of a composite laminate. The behavior of composite laminates containing separation foils was studied in detail both analytically and experimentally. The investigations on three point bending specimens identified that the resulting high deformations between the ends of the sections with separation foils are basically defined by the bending stiffness of the part. The effect of shear was showed to be negligible on resulting deformation.

Moreover, preliminary examinations with –so called- “Donut specimens” proved that the new design concept is easy to apply in practice and brings no deficiencies in terms of strength requirements or manufacturability. Therefore it was decided to use this concept to improve and simplify the current design of the connection elements between the flexbeam and the control cuff of the EC 135 main rotor blades.

5 REFERENCES

- [1] H. Bansemir and S. Emmerling, “*Fatigue substantiation and damage tolerance evaluation of fiber composite helicopter components*“, Applied Vehicle Technology Panel, Corfu-Greece, 1999
- [2] H. Bansemir and K. Pfeifer, “*The damage tolerant design of the EC 135 Bearingless main rotor*“, 24th European Rotorcraft Forum, Marseilles, France, 15-17 September 1998
- [3] H. Bansemir, S. Burghagen and M. Gädke, “*Das Delaminationsverhalten von Unidirektionalverbunden als Grundlage für die Charakterisierung und Dimensionierung von FVW-Strukturen*“, DGLR: Deutscher Luft- und Raumfahrtkongress Friedrichshafen, Germany, 25-29 September 2005

6 ACKNOWLEDGMENT

Special thanks to Dr. H. Bansemir (Eurocopter Germany GmbH).